

# Radio Interferometers with wide bandwidths

Ravi Subrahmanyan

*Australia Telescope National Facility, CSIRO, Locked bag 194, Narrabri, NSW 2390, Australia*

## ABSTRACT

The Australia Telescope Compact Array and the Very Large Array are currently being upgraded to operate with wide bandwidths; interferometers dedicated to the measurement of cosmic microwave background anisotropies are being designed with large instantaneous bandwidths for high sensitivity. Interferometers with wide instantaneous bandwidths that do not operate with correlators capable of decomposing the bands into narrow channels suffer from ‘bandwidth smearing’ effects in wide-field imaging. The formalism of mosaic imaging is extended here to interferometers with finite bandwidths to examine the consequences for the imaging of wide fields if very wide instantaneous bandwidths are used. The formalism presented here provides an understanding of the signal processing associated with wide-band interferometers: mosaicing may be viewed as decomposing visibilities over wide observing bands and, thereby, avoiding ‘bandwidth smearing’ effects in wide-field imaging. In particular, the formalism has implications for interferometer measurements of the angular power spectrum of cosmic microwave background anisotropies: mosaic-mode observing with wide-band radio interferometers decompose wide-band data and synthesize narrow filters in multipole space.

**Key words:** instrumentation: interferometers – methods: observational – techniques: interferometric – cosmic microwave background – radio continuum: general

## 1 INTRODUCTION

When observing continuum radio sources, the sensitivity of a radio interferometer depends on the square root of the bandwidth, apart from other factors. For this reason, arrays are usually designed to have the maximum continuum bandwidths permitted by the state of the art and, additionally, the instantaneous observing bandwidths of existing interferometer arrays are often upgraded over time as the technology associated with sampling rates, transmission bandwidths and correlator speeds improve.

Interferometer arrays that Fourier synthesize images of relatively bright celestial sources are often dynamic range limited owing to artefacts resulting from calibration errors and other systematics; it is in the imaging of the relatively weak sources that thermal noise proves to be the limiting factor. The radio interferometer imaging of cosmic microwave background (CMB) anisotropies, in total intensity and in polarization, is an example of an astrophysical problem where the thermal noise limitation, arising partly from the limited bandwidths in radio interferometers, provides a strong argument in favour of using bolometers – which are intrinsically wide bandwidth devices – for the detection instead of radio interferometers.

Interferometer bandwidths are limited by the state of the technology. If the visibility correlations are to be measured by digital correlators, the wide bandwidth analog signals from the antenna elements would have to be sampled at appropriately high speeds. Interferometers in use today that have the widest bandwidths do not digitise the antenna signals; their correlators are analog multipliers. And an interesting proposal for a dedicated CMB interferometer uses bolometer detectors to measure the interferometer fringe (Ali et al. 2002).

When the celestial source that is being imaged has an intensity distribution over a wide field, or sources distributed over a wide field are being imaged together, wide bandwidth interferometers have special problems and the visibilities suffer from an effect known as ‘bandwidth smearing’ (see, for example, Cotton (1999) and Bridle (1999)). An alternate description of this effect is in Section 2 for the case where a simple two-element interferometer observes sources distributed over a wide field. In Section 3, the formalism of wide-field mosaicing is extended to a wide bandwidth interferometer. The analysis shows that just as mosaic imaging techniques may be adopted for overcoming the limitations posed by the size of the antenna elements, mosaic imaging may also be adopted for overcoming the limitations posed by the size of the bandwidth. Later sections discuss the use of wide bandwidth interferometers in wide field surveys of the sky and measuring the angular power spectrum of CMB temperature anisotropies.

It may be noted here that the ‘bandwidth smearing’ problem in wide-field Fourier synthesis imaging may be avoided by adopting ‘narrow’ bandwidth synthesis or ‘wide’ bandwidth synthesis techniques (Cotton 1999). These methods may not

arXiv:astro-ph/0310240v1 8 Oct 2003

only avoid the problem but also improve the imaging fidelity. However, these bandwidth synthesis methods require that the interferometer correlations be measured separately in multiple frequency channels covering the observing band; in other words, a spectral-line correlator is required for the continuum imaging.

## 2 WIDE FIELD IMAGING

Consider an idealised case where two isotropic antenna elements with infinitesimal effective area, operating at a wavelength  $\lambda$  and corresponding frequency  $\nu = c/\lambda$ , form an interferometer with spacing  $b$ ;  $c$  here denotes the speed of light. The propagation delays in the receiver chains are assumed to have been equalised so that coherent radiation arriving in phase at the two antenna elements will produce a zero-phase interferometer response. The interferometer response, to the brightness distribution over the sky, is the coherence function  $C(s, \nu)$  at the spatial frequency  $s$ , where  $s = b/\lambda$ . The sky brightness distribution results in an EM field on the ground and the measured visibility represents the coherence between the EM fields at the locations of the two antenna elements, this spatial coherence function depends only on the spacing  $b$  and its orientation with respect to the sky and not on the absolute locations of the elements. The coherence function may be expressed as an integral of the sky brightness  $I(\vec{r}, \nu)$  over the celestial sphere:

$$C(\vec{s}, \nu) = \int I(\vec{r}, \nu) e^{-2\pi i(\vec{s} \cdot \vec{r})} d\Omega, \quad (1)$$

where  $\vec{s}$  is the baseline vector:  $\vec{s} = \vec{b}/\lambda$ , and  $\vec{r}$  is a unit vector towards the sky solid angle element  $d\Omega$  (Clark 1999). It is assumed here that the radiation is spatially incoherent across celestial sources and that the sources are extremely distant as compared to the spacing  $b$ .

In the discussions that follow, we assume that the online integration times are sufficiently small, so that ‘time-averaging smearing’ effects are negligible. Additionally, we restrict the imaging to sufficiently small sky regions so that a two-dimensional (2-D) Fourier transform relationship between the sky brightness distribution and the spatial coherence function is a valid approximation. Within this approximation, if the unit vector  $\vec{r}_0$  points towards the interferometer phase centre, and the vector  $\vec{\xi} = (\vec{r} - \vec{r}_0)$  defines offsets from the phase centre,  $\vec{s} \cdot \vec{r}$  in the kernel of equation (1) may be replaced by  $\vec{s} \cdot \vec{\xi}$ .

### 2.1 Effects arising from the use of finite antenna apertures

If the effective apertures of the antennas cover finite areas on the ground, the interferometer response will be an integral of the spatial coherence function over the spatial frequencies sampled by the baseline vectors between elements of one antenna aperture and elements of the other aperture.

To take a specific example, assume that the antennas forming the interferometer have identical circular apertures, uniformly illuminated, with diameter  $d$  and with a spacing  $b$  between their centres. The antenna apertures are assumed to be in the same plane as the interferometer baseline vector and, therefore, the antenna pointing coincides with the interferometer phase centre. The antenna configuration on the ground (real space) is shown in panel *a* of Fig. 1. The interferometer response (measured visibility) is an integral of the spatial coherence function over one of two circular regions, with radius  $d/\lambda$ , of the spatial frequency domain; these circular regions are located symmetrically in the 2-D spatial frequency space with their centres  $b/\lambda$  from the origin. These sampling regions are shown in panel *b* of Fig. 1. The values of the coherence function at points in the spatial frequency plane that are inversion symmetric about the origin are complex conjugates of each other and the implementation of the complex correlator determines the choice of the sampling region. The spatial frequencies are sampled over the range  $(b-d)/\lambda$  to  $(b+d)/\lambda$  with a weighting that linearly decreases from the centres of the circular sampled regions to zero at the edges. For the special case where the antenna apertures are adjacent and  $b = d$ , the coherence function is sampled over the range  $0-2d/\lambda$ .

Interferometers with finite antenna apertures provide visibilities that are integrals over spatial frequency space: the weighted averaging effectively results in a loss of information on the detailed variations of the coherence function over distances in spatial frequency that are smaller than  $2d/\lambda$ . The weighting function in spatial frequency space has a Fourier transform that is the antenna far-field radiation power pattern and, therefore, in the sky domain, the averaging (in spatial frequency space) results in that the interferometer response to brightness away from the antenna pointing centre is attenuated by the primary beam pattern of the antennas. The interferometer does not respond to brightness outside the primary beam and this is a problem for wide-field imaging.

To appreciate better the effect of using antennas with finite-sized apertures, consider the case where a single discrete source is present at a location offset from the centre of the primary beam, which is also the interferometer phase centre. Let the vector  $\vec{\xi} = (\vec{r} - \vec{r}_0)$  define the source position. The spatial coherence function at a location  $\vec{s}$  in spatial frequency domain will have a phase  $-2\pi(\vec{s} \cdot \vec{\xi})$ . Moving along the spatial frequency plane in a direction parallel to  $\vec{\xi}$  (in a direction that has the same direction cosines as  $\vec{\xi}$ ), the phase will wind with period  $(1/\xi)$  wavelengths, where  $\xi$  is the magnitude of the vector offset  $\vec{\xi}$ . The visibility measurements are a weighted average over circular regions of diameter  $2d/\lambda$ , across which the phase

winds ( $2d\xi/\lambda$ ) times. If the source is offset by a distance  $\xi = \lambda/(2d) = c/(2d\nu)$ , the phase of the coherence function winds through  $2\pi$  radians across the sampled circle in spatial frequency domain and the response is severely attenuated. It is this averaging of a rotating coherence function vector, across spatial frequency space, that results in the loss of information on the sky brightness distribution and is usually called the ‘primary-beam attenuation’.

## 2.2 Bandwidth related effects

A baseline vector  $\vec{b}$ , between an element of one of the apertures forming the interferometer and an element of the other antenna aperture, will sample the coherence function at the spatial frequency  $\vec{b}\nu/c$ . Therefore, if the receivers and correlator electronics operate with a finite bandwidth and provide an average visibility measurement over a band covering the range of frequencies  $\pm\Delta\nu$  around a centre frequency  $\nu_0$ , the two elemental apertures with baseline  $\vec{b}$  will average the coherence function over a trace in 2-D spatial frequency space from  $\vec{b}(\nu_0 - \Delta\nu)/c$  to  $\vec{b}(\nu_0 + \Delta\nu)/c$ .

The finite observing bandwidth results in that the measured visibility is an average of the coherence function across spatial frequency space just as the finite apertures result in the visibilities being an average. This averaging across the finite band will result in a loss of information on sky intensity distribution if the traces, corresponding to each pair of elemental apertures, average over a varying coherence function.

In the example we have been considering of an interferometer formed between a pair of circular and uniformly illuminated apertures, the finite bandwidth results in that the circular regions sampled in spatial frequency space scale with increasing frequency. The diameter of the sampled regions scales from  $2d(\nu_0 - \Delta\nu)/c$  at the bottom of the frequency range to  $2d(\nu_0 + \Delta\nu)/c$  at the highest observing frequency. The centre of the circular region also shifts outwards from  $b(\nu_0 - \Delta\nu)/c$  to  $b(\nu_0 + \Delta\nu)/c$ . The movement of the circular sampling region in spatial frequency space, from one end of the observing band to the other, is depicted in panel *c* of Fig. 1.

The averaging of the coherence function in the spatial frequency domain, owing to the finite antenna size, is weighted by a function that is the cross-correlation between the illumination patterns of the two apertures that constitute the interferometer. In the case of identical antennas, the weighting function is the auto-correlation of the illumination, which is also the Fourier transform of the far-field radiation power pattern. The averaging that results from the finite bandwidth is a separate averaging of the coherence function in the spatial frequency domain; in this case the weighting function is defined by the bandpass response of the interferometer. The observed visibility may, therefore, be written as a double integral of the coherence function in spatial frequency space:

$$V(\vec{s}_0) = \int \int \{C(\vec{s}, \nu) W_s(\vec{s} - \vec{s}_0, \nu) d\vec{s}\} W_\nu(\nu - \nu_0) d\nu, \quad (2)$$

where  $\vec{s}_0$  is the baseline vector between the centres of the apertures, in wavelengths, at the centre frequency  $\nu_0$ .  $W_s(\vec{s}, \nu)$  is the auto-correlation of the aperture illumination at frequency  $\nu$  and is, in general, a frequency dependent sampling function in spatial frequency space.  $W_\nu(\nu)$  is the weighting function corresponding to the bandpass shape. The weighting functions are assumed to be normalised so that their integrals are unity.

Consider the coherence function at a baseline  $\vec{b}_0$  owing to a celestial source that is offset from the interferometer phase centre and at a location defined by the vector  $\vec{\xi}$ . Additionally, let the source offset be along the baseline; *i.e.*, let  $\vec{s}_0$ , which is equal to  $\vec{b}_0/\lambda$ , and  $\vec{\xi}$  be vectors with the same direction cosines in their respective planes. The coherence function at this spatial frequency will have a phase  $-2\pi b_0 \nu \xi / c$  and the phase will wind through  $2b_0 \xi \Delta\nu / c$  turns across the band of  $\pm\Delta\nu$ . A source offset by  $c/(2b_0 \Delta\nu)$  will have a coherence function that winds through  $2\pi$  radians across the observing band. It is the loss of information arising from this averaging across the observing band that is called ‘bandwidth smearing’.

The number of phase turns across the observing bandwidth will exceed the number of turns across the visibility space covered by finite apertures if  $(\Delta\nu/\nu_0) > (d/b_0)$ . The averaging length, in spatial frequency space, owing to the finite aperture is proportional to  $d/b_0$  whereas that owing to the finite bandwidth depends on  $\Delta\nu/\nu_0$ . The relative magnitudes of these two quantities decides which effect dominates in any interferometer.

## 3 MOSAICING WITH A WIDE BAND INTERFEROMETER

Scanning the sky with an interferometer, and using the scan data to reconstruct the distribution in the coherence function across the spatial frequencies sampled by the apertures forming the interferometer, was proposed by Ekers & Rots (1979). As far as I know, Rao & Velusamy (1984) were the first to explicitly implement this observing scheme and decompose interferometer visibility data in the spatial frequency domain and then use the finely sampled visibility data to reconstruct wide field images. I extend this formalism below to the case where an interferometer mosaic observes a wide field using a very wide bandwidth.

Consider the case where the arms of a two-element interferometer are phased towards the phase centre  $\vec{r}_0$  and the individual antennas also point towards  $\vec{r}_0$  so that the offset in the pointing of the antennas from the phase centre is zero. The

observed visibility in this case is

$$V(\vec{s}_o, 0) = \int \int \{C(\vec{s}, \nu) W_s(\vec{s} - \vec{s}_o, \nu) d\vec{s}\} W_\nu(\nu - \nu_o) d\nu. \quad (3)$$

When the pointing of the antennas is changed from  $\vec{r}_o$  to  $\vec{r}$ , with the offset denoted by  $\vec{\xi} = (\vec{r} - \vec{r}_o)$ , the coherence function measured between pairs of elements on the two apertures now picks up an additional phase gradient. If the antennas are co-mounted on a common platform, and the pointing as well as phase centres are offset, together, corresponding to the vector  $\vec{\xi}$ , the additional phase is given by

$$\phi(\vec{s}) = 2\pi \{\vec{\xi} \cdot \vec{s}\}. \quad (4)$$

If the antennas are independently mounted, and the interferometer phase centre is kept unchanged, the additional phase acquired at any spatial frequency  $\vec{s}$  is

$$\phi(\vec{s}) = 2\pi \{\vec{\xi} \cdot (\vec{s} - \vec{b}_o \nu / c)\}. \quad (5)$$

In this second case, the signals from the individual antennas may be delayed to introduce a differential delay of  $\tau = (\vec{\xi} \cdot \vec{b}_o) / c$  between the antenna pair with baseline  $\vec{b}_o$ . Then the pointing, delay and phase centres of the independently mounted array would be offset through  $\vec{\xi}$  and the additional phase would be given by equation (4). Assuming that such differential delays are introduced in the case of arrays with independently mounted antennas, the observed visibility is given by (for both mounts)

$$V(\vec{s}_o, \vec{\xi}) = \int \int \{C(\vec{s}, \nu) W_s(\vec{s} - \vec{s}_o, \nu) e^{i2\pi(\vec{\xi} \cdot \vec{s})} d\vec{s}\} W_\nu(\nu - \nu_o) d\nu. \quad (6a)$$

$$= \int \int \{C(\vec{s}, \nu) W_s(\vec{s} - \vec{s}_o, \nu) W_\nu(\nu - \nu_o)\} e^{i2\pi(\vec{\xi} \cdot \vec{s})} d\vec{s} d\nu. \quad (6b)$$

Consider the case where the two-element interferometer scans the sky, moving the pointing of the antennas as well as the phase and delay centres together over a range in offset  $\vec{\xi}$ . This is achieved in the co-mounted case by simply tipping the platform over a range of angles. If the visibilities  $V(\vec{s}_o, \vec{\xi})$  are accumulated over a range of  $\vec{\xi}$  and Fourier transformed to give

$$V(\vec{s}_o, \vec{\chi}) = \int V(\vec{s}_o, \vec{\xi}) e^{-i2\pi(\vec{\xi} \cdot \vec{\chi})} d\vec{\xi}, \quad (7)$$

we obtain

$$V(\vec{s}_o, \vec{\chi}) = \int \int \int \{C(\vec{s}, \nu) W_s(\vec{s} - \vec{s}_o, \nu) W_\nu(\nu - \nu_o)\} e^{i2\pi[\vec{\xi} \cdot (\vec{s} - \vec{\chi})]} d\vec{s} d\nu d\vec{\xi} \quad (8a)$$

$$= \int \left\{ \int C(\vec{s}, \nu) W_s(\vec{s} - \vec{s}_o, \nu) W_\nu(\nu - \nu_o) d\nu \right\} \delta(\vec{s} - \vec{\chi}) d\vec{s} \quad (8b)$$

$$= \left\{ \int C(\vec{s}, \nu) W_s(\vec{s} - \vec{s}_o, \nu) W_\nu(\nu - \nu_o) d\nu \right\} \Big|_{\text{evaluated at } \vec{s}=\vec{\chi}} \quad (8c)$$

$$= \int C(\vec{\chi}, \nu) W_s(\vec{\chi} - \vec{s}_o, \nu) W_\nu(\nu - \nu_o) d\nu. \quad (8d)$$

The  $\delta$ -function above represents the Dirac  $\delta$ -function. The Fourier transformation of the visibility data acquired in different pointings is seen to yield a weighted average of the coherence function. The averaging in equation (8d) is over frequency and not over spatial frequency and, therefore, this method of deriving the visibilities in spatial frequency domain is capable of avoiding the problems associated with band-width smearing related effects.

If the coherence function  $C(\vec{\chi}, \nu)$  is independent of frequency and only a function of the spatial frequency  $\vec{\chi}$ ,

$$V(\vec{s}_o, \vec{\chi}) = C(\vec{\chi}) \int W_s(\vec{\chi} - \vec{s}_o, \nu) W_\nu(\nu - \nu_o) d\nu. \quad (9)$$

In this case, the Fourier transformation of the visibilities that were acquired with the interferometer pointed at different offsets yields weighted samples of the coherence function; the relative weighting depends on the aperture illuminations of the antennas forming the interferometer pair and the bandpass shape.

#### 4 WIDE FIELD IMAGING

In practice, the visibilities  $V(\vec{s}_o, \vec{\xi})$  might be accumulated in a 2-D discrete grid of sky angle offsets spanning a range  $\pm \xi_m$  and with grid size  $\Delta \xi$ . Let this ‘bed-of-nails’ sampling function (a comb of Dirac  $\delta$ -functions) in the sky domain be denoted by  $\Xi(\vec{\xi})$ . For the case where apertures of diameter  $d$  have their centres spaced  $b$  apart, and the observing band is over the

range  $\pm\Delta\nu$ , each complex visibility measurement is composed of spatial frequencies in the range from  $(b-d)(\nu_o - \Delta\nu)/c$  to  $(b+d)(\nu_o + \Delta\nu)/c$ . The complex visibilities (of the real sky) are band limited in the spatial frequency domain to a range of

$$\Delta s = \frac{2(d\nu_o + b\Delta\nu)}{c} = 2\left(d + b\frac{\Delta\nu}{\nu_o}\right)\frac{\nu_o}{c} \text{ wavelengths,} \quad (10)$$

which equals approximately  $2d\nu_o/c$  when the bandwidth is small and  $(\Delta\nu/\nu_o) \ll (d/b)$ . Nyquist sampling, of this signal that is complex and band limited in the spatial frequency domain, requires that

$$\Delta\xi < \frac{c}{2(d\nu_o + b\Delta\nu)}. \quad (11)$$

It may be noted here that if the mosaic observations are made using an interferometer array of antennas, all with diameters  $d$  and observing over a fixed band covering a range  $\pm\Delta\nu$  around a centre frequency  $\nu_o$ , avoiding aliasing in the spatial frequency domain requires that equation (11) be satisfied for the longest baseline.

Explicit transformation of the visibilities  $V(\vec{s}_o, \vec{\xi})$  into visibilities  $V(\vec{s}_o, \vec{\chi})$  distributed over the spatial frequency range given by equation (10) is possible using equation (9) provided that the Nyquist sampling criterion is satisfied. The discrete Fourier transformation (DFT) of the visibilities  $V(\vec{s}_o, \vec{\xi})$ , which are discrete samples in offset  $\vec{\xi}$  space, would yield samples of the visibility  $V(\vec{s}_o, \vec{\chi})$  in spatial frequency. If the mosaic grid measures  $2\xi_m/\Delta\xi$  complex visibilities along any sky dimension, the DFT would yield  $2\xi_m/\Delta\xi$  independent measures of the complex visibility in the conjugate space which is the spatial frequency  $\vec{\chi}$  domain. Samples spaced  $1/(2\xi_m)$  wavelengths apart would be independent. These visibility samples are weighted averages of the coherence function in spatial frequency domain with a point spread function (PSF) that is determined by the sampling in  $\vec{\xi}$  space and is independent of the bandwidth; the samples  $V(\vec{s}_o, \vec{\chi})$  are essentially averages of the coherence function over spatial frequency ranges that are  $1/(2\xi_m)$  wavelengths wide.

The implication here is that even if the observing bandwidth is large, and in the extreme case if  $(\Delta\nu/\nu_o)$  exceeds  $(d/b)$  so that the attenuation owing to bandwidth smearing exceeds the primary beam attenuation in the individual fields, mosaicing observations with a sampling that satisfies equation (11) can image large fields of view. The DFT to spatial frequencies would decompose the observed visibilities – that are integrals of the coherence function over wide spatial frequency ranges corresponding to the wide bandwidths used – into samples that correspond to regions that are effectively  $1/(2\xi_m)$  wavelengths wide. *Just as mosaicing has the ability to decompose the observations made with wide-aperture antennas into visibilities corresponding to those obtained with small aperture arrays, mosaic mode observing has the ability to decompose the visibilities made with wide bandwidths into those corresponding to narrow bands.*

The DFT to spatial frequencies decomposes the observed visibilities into  $1/(2\xi_m)$  wavelength wide bins and, as stated above, these visibilities  $V(\vec{s}_o, \vec{\chi})$  are samples of the coherence function, weighted by functions that are defined by the aperture illumination and bandpass shape, and convolved by a PSF  $\Xi'(\vec{\chi})$  that is the Fourier transform of the sampling function  $\Xi(\vec{\xi})$ :

$$V(\vec{s}_o, \vec{\chi}) = \left\{ C(\vec{\chi}) \int W_s(\vec{\chi} - \vec{s}_o, \nu) W_\nu(\nu - \nu_o) d\nu \right\} \otimes \Xi'(\vec{\chi}), \quad (12)$$

where the operator  $\otimes$  denotes convolution. The weighting function

$$W_{s\nu}(\vec{\chi}) = \int W_s(\vec{\chi} - \vec{s}_o, \nu) W_\nu(\nu - \nu_o) d\nu \quad (13)$$

is computable from the aperture illuminations of the antennas forming the interferometer pair and the bandpass shape,  $\Xi'(\vec{\chi})$  is also computable from the adopted mosaic grid on the sky. In terms of these known functions, the derived visibilities may be expressed in the form

$$V(\vec{s}_o, \vec{\chi}) = \{C(\vec{\chi})W_{s\nu}(\vec{\chi})\} \otimes \Xi'(\vec{\chi}). \quad (14)$$

Samples of these visibility estimates, which are separated by  $1/(2\xi_m)$  wavelengths, are independent and may be used to reconstruct images of the sky. These images are that of the true sky intensity distribution convolved by a PSF that is the Fourier transform of the weights  $W_{s\nu}(\vec{\chi})$ . The image would be tapered by the DFT of  $\Xi'(\vec{\chi})$ , which is simply the top-hat function  $\Xi(\vec{\xi})$  that encompasses the entire sky area covered by the mosaic pattern.

## 5 THE POWER SPECTRUM OF CMB ANISOTROPIES

Assuming that the sky temperature anisotropies in the CMB are Gaussian random fluctuations with random phase, they may be completely described by the  $C_l$  coefficients of spherical harmonic decompositions. Observations of CMB anisotropies attempt to measure the angular power spectrum, which is the distribution of  $l(l+1)C_l/(2\pi)$  over multipole  $l$  space.

The  $C_l$  coefficient represents the anisotropy power at multipole mode  $l$  and in the limit of large  $l$  and small sky angles, the spherical harmonic decomposition approximates to a Fourier decomposition and the distribution of anisotropy power over  $l$  space is simply related to the distribution of the variance in observed visibilities over spatial frequencies. A spatial

frequency  $s_o$  corresponds to a multipole mode  $l_o = 2\pi s_o$  and the variance in CMB visibilities that are measured over a band  $\Delta s$  is a measure of the CMB anisotropy over a multipole range  $\Delta l = 2\pi\Delta s$ . Interferometer measurements of CMB anisotropy hence provide estimates of  $C_l$  power in which the telescope filter functions are defined by the aperture illuminations of the antennas and the projected baseline length. If the interferometer mosaic images a wide field, these visibility data at multiple pointings might be used to derive visibilities corresponding to narrow filters in spatial frequency space. Therefore, mosaic mode observations are a method for decomposing the interferometer  $C_l$  measurements into those corresponding to narrow telescope filter functions in  $l$  space: mosaic observing improves  $l$ -space resolution (White et al. 1999; Subrahmanyan 2002). Moreover, it has been argued that drift scanning the sky, using a co-mounted antenna array operated as interferometers, is a useful technique for rejecting systematics (Subrahmanyan 2002); drift scanning is an implementation of the mosaicing technique.

Towards any single pointing, a wide bandwidth interferometer samples a range in  $l$  space and the anisotropy variance is averaged over this range to produce the interferometer response. When a wide-band interferometer observes CMB anisotropies over a wide field in mosaic mode, as discussed in the preceding sections, the visibilities obtained in the multiple pointings may be transformed to yield visibilities distributed in spatial frequency  $\chi$ . In the small angle approximation where  $\vec{l} = 2\pi\vec{\chi}$ ,  $V(\vec{s}_o, \vec{l}) = \{C(\vec{l})W_{s\nu}(\vec{l})\} \otimes \Xi'(\vec{l})$ . (15)

The variance in  $V(\vec{s}_o, \vec{l})$  is an estimate of the anisotropy power at multipole order  $l = |\vec{l}|$  and this is independent of the instantaneous bandwidth of the interferometer. The mosaic mode effectively decomposes the measurements that are averages over wide bandwidths – and, consequently, averages over wide  $l$ -space domains – into narrow  $l$ -space filters that are defined by  $\Xi'(\vec{l})$ .

## 6 SENSITIVITY CONSIDERATIONS

Consider the case where a two-element interferometer, consisting of apertures of diameter  $d$  and baseline  $b$ , observes an  $n \times n$  mosaic of pointings for a total time  $t$  (the time spent at each pointing is  $t/n^2$ ). Assume first that the observations are made using a narrow bandwidth  $(\Delta\nu/\nu_o) \ll (d/nb)$ . Assume further that the pointings are separated by the required Nyquist rate of  $(c/2d\nu_o)$ . The signal to noise ratio (SNR) in the measurement of the flux density of a point source that appears in any one of the pointings will be proportional to  $d^2\sqrt{t}/n$ . If, instead, this interferometer that is formed of apertures of diameter  $d$  observes the source position for the entire time  $t$ , the SNR would be proportional to  $d^2\sqrt{t}$ .

If the interferometer consisted of a pair of apertures of size  $d/n$  and the entire field were observed as a single pointing for the same total time  $t$ , the SNR would be proportional to  $d^2\sqrt{t}/n^2$ . Using  $n^2$  such apertures with diameter  $d/n$  and simultaneously measuring  $n^2$  correlations recovers the SNR that is proportional to  $d^2\sqrt{t}/n$ . If an array consisting of  $2 \times n^2$  such apertures were used, with a total collecting area corresponding to the area of the two-element interferometer with apertures of diameter  $d$ , and if all  $n^4$  correlations were simultaneously measured, the SNR would increase further and be proportional to  $d^2\sqrt{t}$ . This last value is the same as that expected in the case where a two-element interferometer with apertures of diameter  $d$  observes a source for the entire time  $t$ ; however, the observation with apertures of size  $d/n$  provides this high sensitivity over the entire mosaic field which is larger by factor  $n \times n$ .

If the fractional bandwidth exceeds  $d/(nb)$  – so that bandwidth smearing effects are significant over the wide mosaiced field – but if the constraint  $(\Delta\nu/\nu_o) \ll (d/b)$  is satisfied, mosaic observations of the wide field using the  $d$ -sized apertures and covering the wide field in  $n \times n$  pointings would not be compromised in sensitivity. However, non-mosaiced observations of the wide field using  $d/n$ -sized apertures and the wide bandwidths would suffer from bandwidth smearing effects.

If  $(\Delta\nu/\nu_o) \gtrsim (d/b)$ , the number of mosaic pointings would have to be significantly increased. If  $(\Delta\nu/\nu_o) = k(d/b)$ , the pointing grid size  $\Delta\xi$  would have to be reduced by factor  $(1+k)$ . A mosaic observation using a two-element interferometer consisting of apertures of diameter  $d$ , covering a grid of size  $n(1+k) \times n(1+k)$ , would detect point sources in the wide field with a

$$\text{SNR} \propto \left(\frac{d^2\sqrt{t}}{n}\right) \frac{\sqrt{k}}{(1+k)}. \quad (16)$$

This SNR has a maximum at  $k = 1$  corresponding to the case where  $(\Delta\nu/\nu_o) = (d/b)$  and the mosaic is made with a grid size on the sky of

$$\Delta\xi = \frac{c}{4d\nu_o}. \quad (17)$$

The analysis suggests that when interferometers with wide instantaneous bandwidths are used for the mosaic imaging of wide fields, including the particular case of mosaic-mode CMB observations, the optimum bandwidth corresponds to the case where  $(\Delta\nu/\nu_o) = (d/b)$ ; the SNR degrades if the instantaneous bandwidth used exceeds  $(2d/b)\nu_o$ .

Interferometers with wide fractional bandwidths are of particular interest at high frequencies where errors due to telescope pointing and interferometer phase may be significant. therefore, the limitations arising from such errors are considered below.

Any systematic pointing error of magnitude  $\epsilon_p$  in the antennas forming the wide-bandwidth interferometer would result in phase errors in the complex visibilities following the decomposition in spatial frequency space. These errors would vary across spatial frequencies and lie in the range  $(\epsilon_p/\theta_{\nu_0-\Delta\nu})$  to  $(\epsilon_p/\theta_{\nu_0+\Delta\nu})$ , where  $\theta_\nu$  is the FWHM of the primary beam at frequency  $\nu$ . The limiting factors to the quality of mosaic images made using interferometer arrays was discussed by Cornwell, Holdaway & Uson (1993) for the case where the visibility was obtained in narrow bands. In the case of mosaic imaging with a wide bandwidth interferometer, the image fidelity (defined as the ratio of the value of an image pixel to the error between the true sky and reconstructed image) is, in particular, limited by telescope pointing errors. The fidelity is limited approximately to

$$\Lambda^{PE} \approx \frac{\sqrt{N_A}\theta_{\nu_0}}{\epsilon_p \left(1 + \frac{b\Delta\nu}{d\nu_0}\right)}, \quad (18)$$

where  $\theta_{\nu_0}$  is the FWHM of the primary beam at frequency  $\nu_0$ ,  $N_A$  is the number of antenna elements in the array and  $\epsilon_p$  is the systematic pointing error associated with any antenna; it is assumed that the errors are uncorrelated between antennas.

Mosaic scanning is also limited by time varying phase errors that introduce a varying phase error over the sky scans. If  $\epsilon_\phi$  is the R.M.S. phase error (in radians) during the scanning then the visibility amplitudes following the decomposition in spatial frequency space would have fractional errors of order  $\epsilon_\phi$ . In the case of interferometer mosaic imaging, assuming that these errors are antenna based (as would be expected for atmospheric phase errors), the image plane fidelity would be approximately limited by these errors to  $N_A/\epsilon_\phi$ .

## 7 SUMMARY

Wide band interferometers – in which the band is not finely sub-divided in multi-channel receivers – instantaneously sample a wide domain in spatial frequency space. Mosaic imaging of wide fields, which are made by covering the wide fields with a grid of pointings and subsequently transforming the visibilities that are measured in the multiple pointings to visibility space, yields samples of the visibilities distributed in the spatial frequency domain. The formalism of mosaic imaging of wide fields has been extended here to the case where the interferometers operate with wide instantaneous bandwidths. The mosaicing technique may be viewed as effectively decomposing wide-band data into spatial frequency bins. The formalism presented here develops the understanding of the mosaicing technique that reconstructs wide-field images without ‘bandwidth smearing’ effects.

The signal-to-noise ratio in a mosaicing interferometer improves as the bandwidth is increased; however, the usefulness of the wide band for wide-field imaging diminishes once the bandwidth exceeds  $(2d/b)\nu_0$ . Admittedly, a multi-channel receiver improves upon the sensitivity of the mosaicing interferometer; however, the gain is marginal if the total band is less than  $(2d/b)\nu_0$ . The considerations discussed here are relevant both to the case where the mosaicing interferometer attempts to reconstruct sky images and to the case where the mosaicing interferometer attempts a measurement in spatial frequency space of the angular power spectrum of the sky brightness fluctuations.

## ACKNOWLEDGMENTS

This work was stimulated by discussions with members of the Taiwanese AMiBA CMB project.

## REFERENCES

- Ali S., Rossinot P., Piccirillo L., Gear W. K., Mausekopf P., Ade P., Haynes V., Timbie P., 2002, in De Petris M., Gervasi M., eds, AIP Conf Proc. Vol. 66, Experimental Cosmology at Millimetre Wavelengths, AIP, New York, p. 126
- Bridle A. H., Schwab F. R., 1999, in Taylor G. B., Carilli C. L., Perley R. A., eds, ASP Conf Ser. 180, Synthesis Imaging in Radio Astronomy II, ASP, San Francisco, p. 371
- Clark B. G., 1999, in Taylor G. B., Carilli C. L., Perley R. A., eds, ASP Conf Ser. 180, Synthesis Imaging in Radio Astronomy II, ASP, San Francisco, p. 1
- Cornwell T. J., Holdaway M. A., Uson J. M., 1993, A&A, 271, 697
- Cotton W. D., 1999, in Taylor G. B., Carilli C. L., Perley R. A., eds, ASP Conf Ser. 180, Synthesis Imaging in Radio Astronomy II, ASP, San Francisco, p. 357
- Ekers R. D., Rots A. H., 1979, in van Schooneveld C., eds, Astrop. & Sp. Sc. Lib. 76, Image Formation from Coherence Functions in Astronomy, Reidel, Dordrecht, p. 61
- Rao A. P., Velusamy T., 1984, in Roberts J. A., eds, Indirect Imaging, Cambridge Univ. Press, Cambridge, p. 193
- Subrahmanyan R. 2002, in Chen L. -W., Ma C. -P., Ng K. -W., Pen U. -L., eds, ASP Conf Ser. 257, AMiBA 2001: High-z Clusters, Missing Baryons, and CMB Polarization, ASP, San Francisco, p. 309
- White M., Carlstrom J. E., Dragovan M., Holzzapfel W., 1999, ApJ, 514, 1

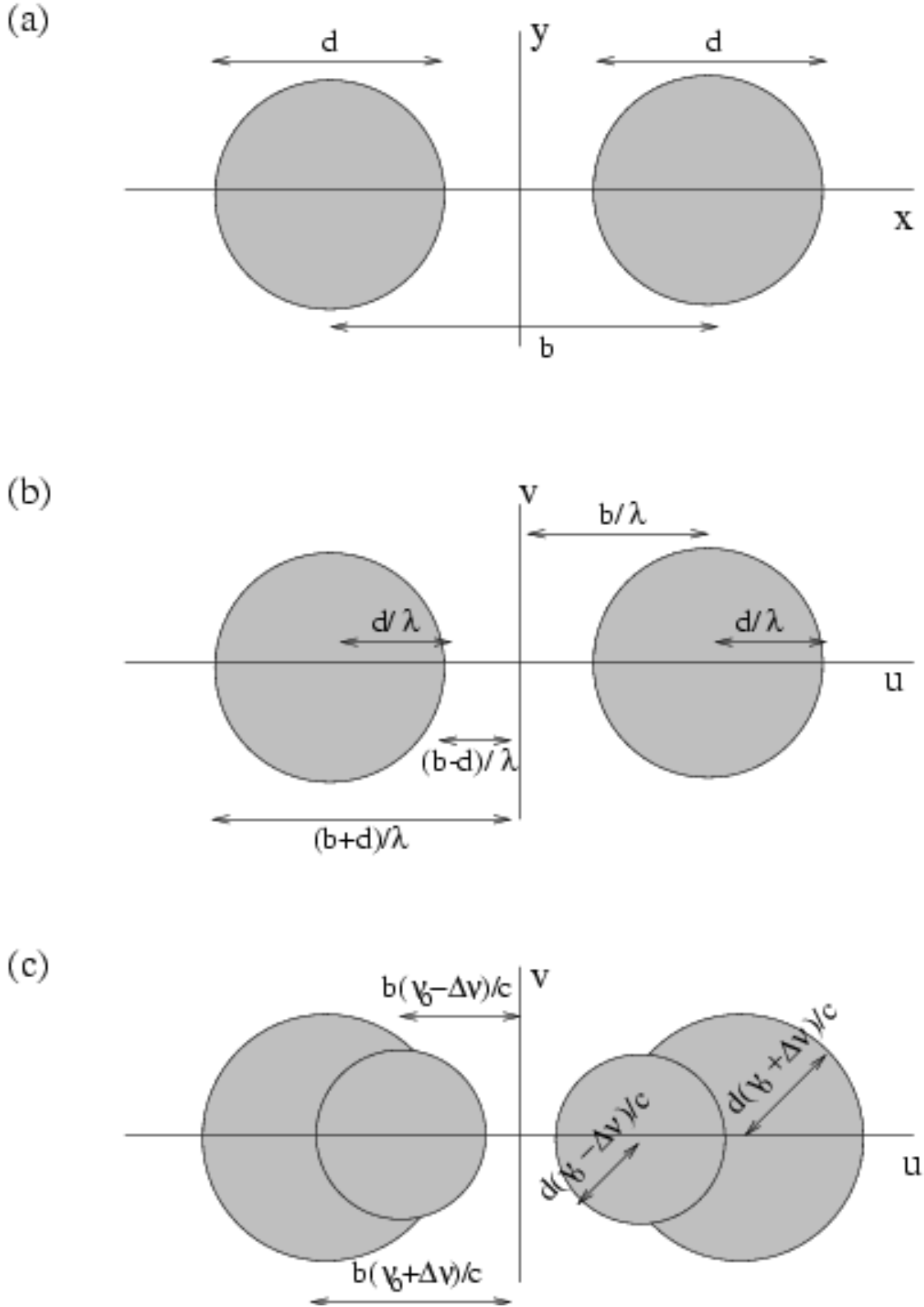


**Figure 1.** Panel *a* shows the configuration and dimensions of the aperture elements forming the interferometer in real space. Panel *b* shows the visibility sampling in spatial frequency space. Panel *c* shows the change in the sampling of the spatial frequency domain across the observing band.